High-Resolution Dynamic Pressure Sensor Array Based on Piezo-phototronic Effect Tuned Photoluminescence Imaging

Mingzeng Peng,[†,⊥] Zhou Li,[†,∥,⊥] Caihong Liu,[†] Qiang Zheng,[†] Xieqing Shi,[†] Ming Song,[†] Yang Zhang,[†] Shiyu Du,[§] Junyi Zhai,[*,†] and Zhong Lin Wang[*,†,‡]

[†]Beijing Institute of Nanoenergy and Nanosystems, Chinese Academy of Sciences, Beijing 100083, China, [‡]School of Materials Science and Engineering, Georgia Institute of Technology, Atlanta, Georgia 30332-0245, United States, [§]Division of Functional Materials and Nanodevices, Ningbo Institute of Materials Technology and Engineering, Chinese Academy of Sciences, Ningbo, Zhejiang 315201, China, and [∥]Key Laboratory for Biomechanics and Mechanobiology of Ministry of Education, School of Biological Science and Medical Engineering, Beihang University, Beijing 100191, China. [⊥]These authors contributed equally to this work.

ABSTRACT A high-resolution dynamic tactile/pressure display is indispensable to the comprehensive perception of force/mechanical stimulations such as electronic skin, biomechanical imaging/analysis, or personalized signatures. Here, we present a dynamic pressure sensor array based on pressure/strain tuned photoluminescence imaging without the need for electricity. Each sensor is a nanopillar that consists of InGaN/GaN multiple quantum wells. Its photoluminescence intensity can be modulated dramatically and linearly by small strain (0−0.15%) owing to the piezo-phototronic effect. The sensor array has a high pixel density of 6350 dpi and exceptional small standard deviation of photoluminescence. High-quality tactile/pressure sensing distribution can be real-time recorded by parallel photoluminescence imaging without any cross-talk. The sensor array can be inexpensively fabricated over large areas by semiconductor product lines. The proposed dynamic all-optical pressure imaging with excellent resolution, high sensitivity, good uniformity, and ultrafast response time offers a suitable way for smart sensing, micro/nano-opto-electromechanical systems.

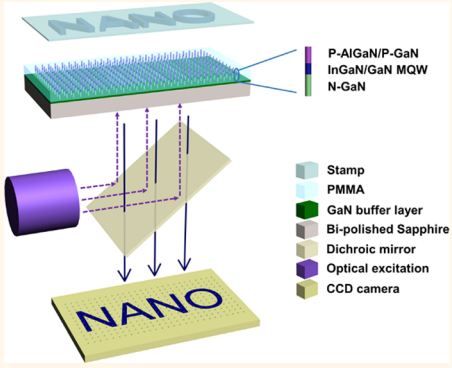

KEYWORDS: all-optical devices · dynamic pressure sensors · piezo-phototronics · photoluminescence · smart skin

Smart sensing, such as emulating electronic skin and human−computer interfacing, offers new opportunities in sensor networks for artificial intelligence to carry out identification, positioning, tracking, monitoring, communication, and management. The design, fabrication, and realization of large-scale, dynamic, high-resolution pressure-sensitive arrays are indispensable to further promote the comprehensive perception of pressure/strain, position, and motion. Nowadays, the pressure sensor arrays, made from microstructured rubber layers,[1] assembled nanowires or nanotubes,[2−4] or transistors,[5−7] are based on a change of electrical signal such as capacitance or resistance under applied pressure. However, to get a two-dimensional (2D) image of pressure distribution,[1−7] each independent device element in the cross-bar electrodes has to be connected to the measurement circuit one by one. Therefore, the increased number of pixels will dramatically decrease the response speed of the 2D electrical array device. Furthermore, another alternative method is using an optical readout signal for pressure imaging by electro-optical conversion, which aims to achieve user-interactive pressure/tactile visualization.[8,9] Even so, an electrical interconnect layout for a high-density matrix increases fabrication complexity and current maldistribution. Thus, it is hard to simultaneously achieve large-area, high-density, and high-speed imaging for pressure sensing distribution.

Until now, the advance of all-optical devices has greatly promoted the speed and capacity of information communication

* Address correspondence to jyzhai@binn.cas.cn, zlwang@gatech.edu.

Received for review January 5, 2015 and accepted February 24, 2015.

Published online February 24, 2015
10.1021/acsnano.5b00072

technology.[10] The demonstrations of all-optical functional components, such as switches,[10,11] memories,[12,13] modulators,[14,15] and regenerators,[16] open up the feasibility of on-chip photonic integration or networks. In particular, utilizing all-optical imaging for smart sensing can be a novel and suitable way for large-area, highly uniform, high-resolution sensing applications. The elimination of an electrode greatly reduces the device complexity of 2D matrix arrays and helps large-scale and high-density integration for high-resolution active sensing at the micrometer or submicrometer level. In addition, no electrical injection drastically reduces power consumption. More importantly, the self-heating effect in electronic devices could be completely avoided, which is a common problem for long-term reliability in poor thermal conductivity materials. Furthermore, in large-scale matrix arrays, it is noted that nonuniform current spreading phenomenon[17] directly worsens the spatial distribution of an electric field or electroluminescence and device stability in optoelectronic imaging.

As an all-optical method, photoluminescence (PL) has been widely used for analyzing the electronic structure of materials such as band gaps, crystal structure, impurity levels, and defects. Although a few papers reported strain-induced change of the band gap and PL in semiconductor nanowires (Ge, GaAs),[18,19] such modulation only occurred under a very large strain. Here, we present that PL intensity of InGaN/GaN multiple quantum well (MQW) can be tuned dramatically and linearly by a small strain (0−0.15%) due to the piezo-phototronic effect for the first time. On this basis, a new type of all-optical pressure sensor array was designed without the need for electricity. Each pressure sensor is a nanopillar that consists of vertically aligned InGaN/GaN MQWs. The sensor array was top-down fabricated inexpensively over large scales. Most importantly, dynamic pressure distribution mapping has been successfully achieved by the ultrafast pressure/strain-sensitive PL imaging, which demonstrates potential applications in biomechanical imaging/analysis, next-generation touch-pad technology, personalized signatures, identity authentication, human−machine interfacing, micro/nano-opto-electromechanical systems, *etc.*

RESULTS AND DISCUSSION

Figure 1 shows a schematic diagram of a pressure-sensitive PL imaging measurement system. Our device is based on vertically aligned InGaN/GaN MQW nanopillar arrays. Each pillar works as an independent pressure-sensitive sensor. The basic structure of each sensor contains n-GaN, five light-absorbing InGaN/GaN QWs, and p-AlGaN/p-GaN layers. To optimize optical absorption and transition of $In_{0.18}Ga_{0.82}N$/GaN MQW nanopillars used in this work, the wavelength of excitation in the optical source was chosen to be 405 nm.

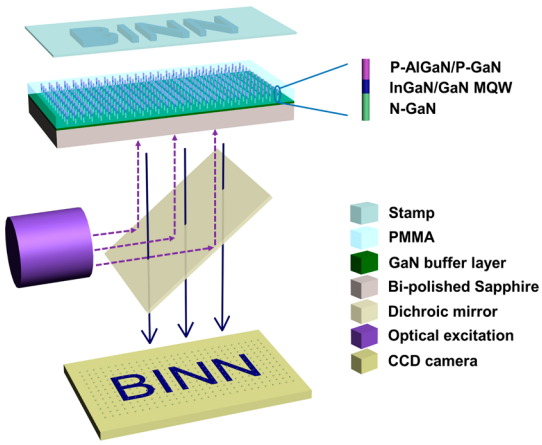

Figure 1. Schematic diagram of piezo-phototronic effect tuned PL imaging. The pressure sensor array is based on vertically aligned pillars that consist of InGaN/GaN MQWs. The basic structure of each sensor contains n-GaN, five light-absorbing InGaN/GaN QWs, and p-AlGaN/p-GaN layers. When applying pressure/strain by a pressure stamp with a BINN pattern, a high-resolution PL image of BINN is depicted in the spatial pressure distribution in real time.

The incident photons can penetrate through the bipolished sapphire substrate and GaN layer and then be absorbed by $In_{0.18}Ga_{0.82}N$ QW layers of each pillar. The generated PL imaging can be read in real time. In addition, a pressure stamp with a "BINN" pattern was fabricated for pressure-sensitive imaging measurement by using a negative photoresist SU-8 mold. The InGaN/GaN MQW nanopillars that contacted the convex part of the pressure stamp were compressed along the *c*-axis direction, leading to the generated pressure-induced negative and positive piezoelectric charges in their top and bottom parts.[20,21] Under compressive force/strain, piezoelectric polarization charges increased the internal electric field of the InGaN/GaN MQW active region at the p−n junction and tuned the charge separation, transportation, and/or recombination[22−28] in the PL mechanisms. Meanwhile, the non-compressed nanopillars had no piezoelectric-induced charges, thus no change of PL intensity could be found from these nanopillars. In addition, it is noted that the PL dynamic process takes place at a very short time of nanoseconds or less,[29,30] which is beneficial for fast-speed optical imaging. By using a charge-coupled device (CCD) to collect and monitor the PL intensity of all sensors, the all-optical imaging of the applied pressure distribution can readily be attained.

The sensor array was simply achieved by the state-of-the-art top-down fabrication from an epitaxial InGaN/GaN multilayer on a *c*-plane bipolished sapphire substrate,[22] including a photolithography patterned nickel−metal dot matrix (Figure 2a), low-damage dry etching of GaN-based thin films (Figure 2b), and removal of the Ni−metal mask (Figure 2c). It should be noted that no extra electrodes were needed here, which dramatically reduced the process complexity and extremely cut down the fabrication cost. As shown

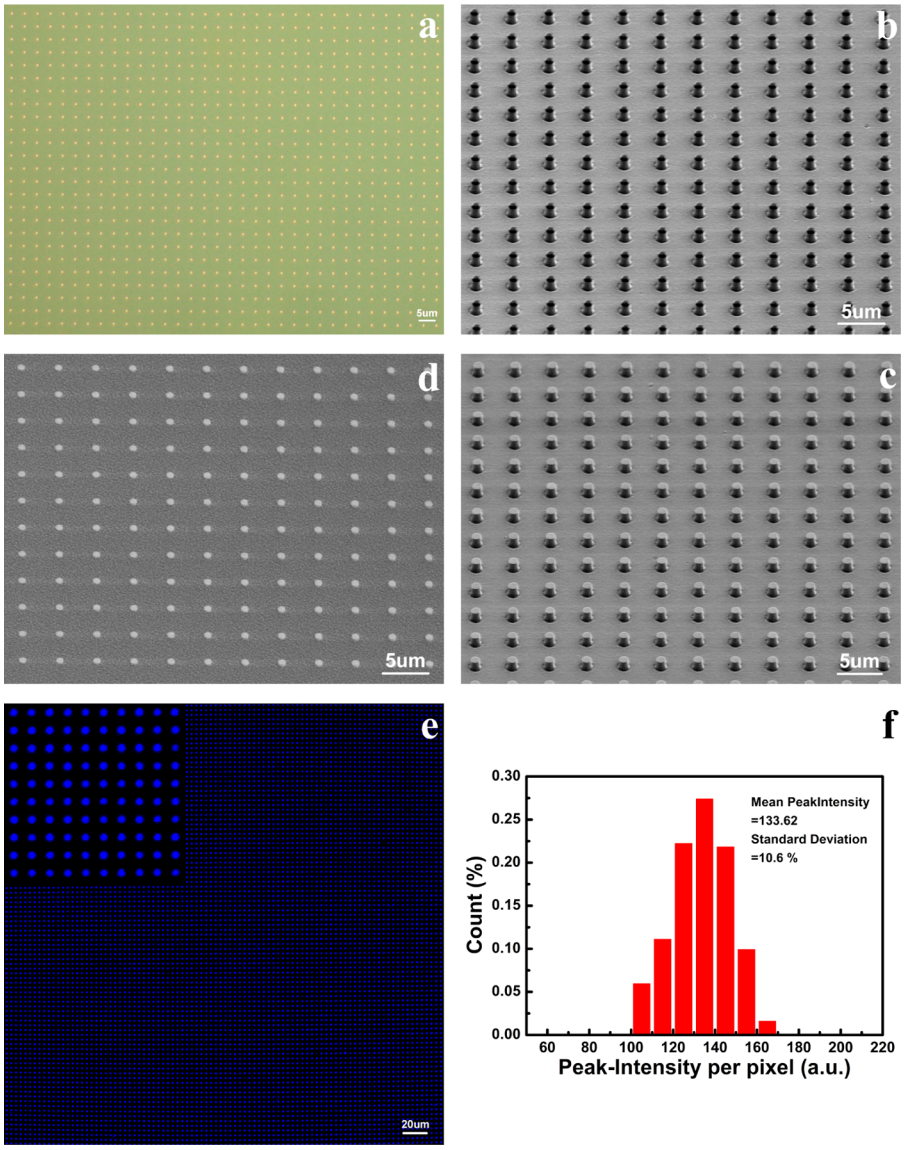

Figure 2. Top-down device fabrication and PL imaging. (a) Large-area, well-ordered nickel−metal dot matrix fabricated by photolithography patterning, metal evaporation, and lift-off processes. (b) Low-damage dry etching of GaN-based thin films patterned by nickel−metal dot matrix. (c) MQW pillar array after removing the Ni−metal mask. (d) Visibly transparent PMMA polymer spin-coated to fill in the pillar array, the clean tips of which are exposed by oxygen plasma etching. (e) Corresponding PL signals of our MQW pillar array, in parallel emitted at a peak wavelength of ~460 nm. (f) Statistical results of the PL peak intensities of all blue-light pixels in (e).

in Figure 2, the well-aligned and uniform InGaN/GaN nanopillar array has a density of 6.25×10^6 cm^{-2}. The diameter, height of each pillar, and distance between two adjacent pillars are 0.8, 1.2, and 4 μm, respectively. Such vertically aligned nanopillar arrays could be fabricated in a large area with excellent uniformity of size, shape, period, and height by this top-down fabrication technique. The extremely small variance in the height of all pillars ensures a clearly defined and reproducible top contact plane for pressure sensing. A visibly transparent poly(methyl methacrylate) (PMMA) polymer was used to completely fill in our array, the tips of which were exposed by oxygen plasma etching as shown in Figure 2d. This flattened composite structure can greatly improve the mechanical robustness of our nanoarray device, especially for dynamic pressure sensing.

Based on the PL excitation method, the large-area, highly bright InGaN/GaN MQW nanopillar array was uniformly lit up by a laser diode of 405 nm, which can be substituted by other wide-spectrum violet or ultraviolet light sources. Its corresponding PL signals, in parallel emitted at a peak wavelength of ~460 nm, were collected in Figure 2e by a thermoelectrically cooled CCD detector. Figure 2e shows a large-area uniform distribution of the emitted blue PL from our high-density pillar array, which can reach the PL imaging area of several square centimeters without the view-field limitation of the objective lens and CCD camera. Each pixel is a blue-light emitter. The period

of the blue-light spot matrix is 4 μm, corresponding to a high pixel resolution of 6350 dpi. It is noted that the diameter of the light spot is only 1.2 μm with a highly centralized distribution of light intensity, the size of which is just slightly bigger than that of the MQW pillar in Figure 2c. No cross-talk takes place between any adjacent blue-light spots. Therefore, it guarantees a better spatial resolution for pressure imaging compared to the electroluminescent method reported previously.[9] Furthermore, the PL peak intensities of all blue-light spots are statistically calculated in Figure 2f. The mean PL peak intensity and corresponding standard deviation are 133.62 and 10.6%, respectively, demonstrating that the PL from the sensor array is highly uniform. As a result, our top-down fabricated InGaN/GaN MQW pillar array exhibits a large-area, high-resolution, no cross-talk PL imaging.

Figure 3a shows the PL spectra of the MQW nanopillar array at different power densities of the excitation light source from 2 to 20 mW/mm^2 at room temperature. The PL intensity increased with increasing excitation optical power. However, the PL emission peak was constant at around 460 nm from the light emission of InGaN QW layers. It is worth mentioning that the in-plane residual strain in InGaN/GaN MQW nanopillars has been greatly relaxed after top-down fabrication.[31]

For the pressure/stress dependence of the PL spectra, various external compressive stresses were applied to our pressure sensor array, which were measured by force gauge. Since the MQW nanopillar only occupied a very small portion of the pressure sensing area, the external stress exerted on the sensor array (σ_s) is much smaller than that applied on the MQW pillars (σ_p). The pressure magnification factor (M) can be calculated by $M = \sigma_p/\sigma_s = a_s/a_p$, where a_s and a_p are the cross-sectional areas of the sensor unit and each pillar in Figure S1, respectively. According to our array structure, the value of the M factor is 31.83. In addition, Figure 3b presents the PL spectra of a typical MQW pillar from 420 to 513 nm under different compressive stresses. It is noted that its emitted PL intensity can be strongly modulated by the magnitude of the applied external pressure up to 14.94 MPa (corresponding to the pillar's strain of ~0.15%), while almost keeping its PL peak wavelength the same. Therefore, we mainly focused on its relative PL intensity change ($|L_\sigma - L_0|/L_0$) as a function of the applied compressive stress σ_s, the relationship of which is presented in Figure 3c, where L_σ and L_0 denote the integral PL intensity between 420 and 513 nm under the applied stress and zero stress, respectively. The external pressure/stress was exerted on our array by the patterned BINN stamp. The InGaN/GaN MQW nanopillars, which were in contact with the BINN stamp, were deformed when applying the stresses and *vice versa*. At the deformed region, there exists a nearly linear increase of the PL intensity change with the external stress, while there is only a slight

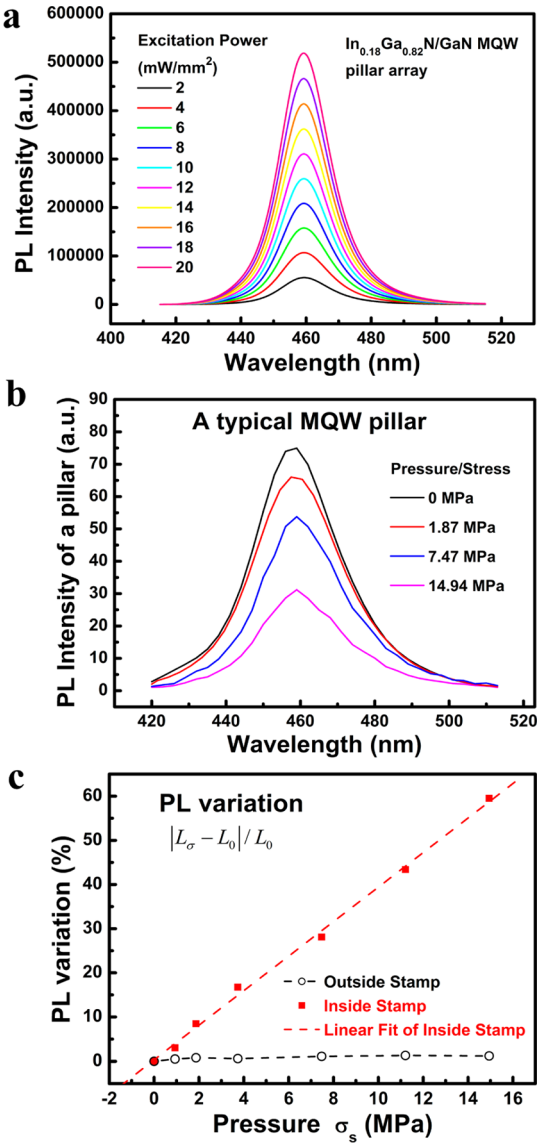

Figure 3. PL characterization of our MQW pillar array. (a) PL spectra of the MQW pillar array at different power densities of the excitation light source from 2 to 20 mW/mm^2 at room temperature. (b) PL spectra of a typical MQW pillar under various compressive stresses. (c) Changes of PL intensity inside and outside the BINN stamp as a function of the applied compressive stress.

fluctuation at the nondeformed region, as shown in Figure 3c. The pressure sensitivity (S) of our InGaN/GaN MQW nanopillar array is defined as[1]

$$S = \frac{\delta(\Delta L/L_0)}{\delta\sigma_s} = \frac{\delta(|L_\sigma - L_0|/L_0)}{\delta\sigma_p} \times \frac{a_s}{a_p} \qquad (1)$$

The sensitivity can be derived from the slope of the relationship between the PL intensity change and the applied stress in Figure 3c. It is proportional to the pressure magnification factor M. For our pillar array, the S value of 39.09 GPa^{-1} remains keeps the same from low pressure to 15 MPa, which gives >3-fold improvement in pressure sensitivity compared with the results reported before.[9] At ~2 MPa pressure level,

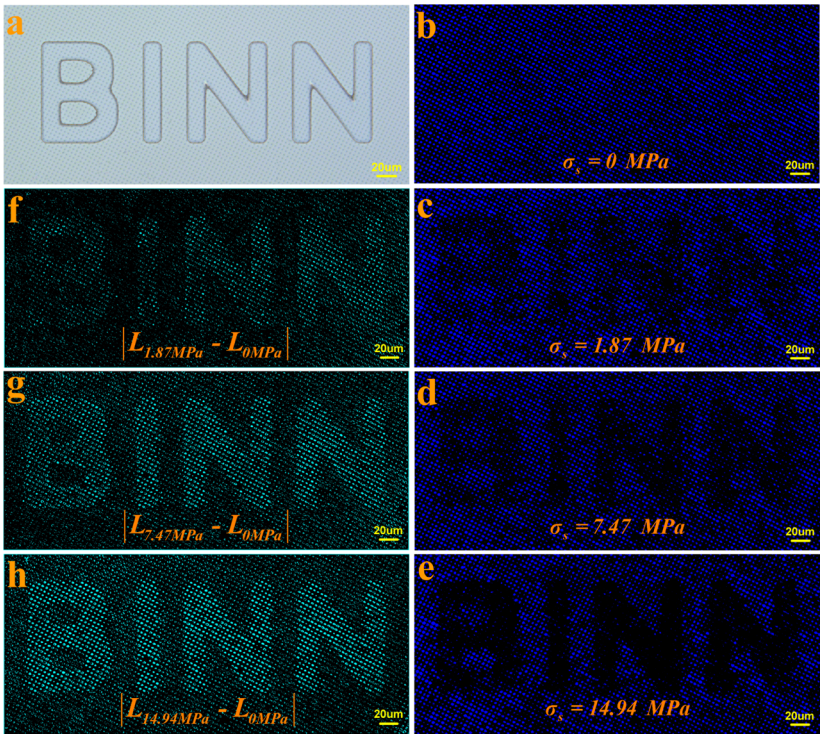

Figure 4. High-resolution PL imaging of pressure/strain distribution. (a) Bright-field image of the BINN stamp in contact with the MQW pillar array. (b−e) Static PL images of the MQW nanopillar array by pressing the BINN stamp under different pressure/stresses of 0, 1.87, 7.47, and 14.94 MPa, respectively. (f−h) Two-dimensional PL intensity differential images derived from PL maps (b−e) by numerical subtraction, respectively.

a high-resolution pressure image of the BINN logo is also clearly observed in Figure 4c. It has to be noted that the pressure sensitivity can be further increased by partially lowering the array resolution or decreasing the size of the pillar. If the resolution of the nanopillar array is changed to the same resolution as human skin (~50 μm),[32] the pressure sensing will be enhanced to the level of ~12.8 kPa, which is in the medium-pressure regime (10−100 kPa). Besides, the pressure sensitivity will reach 6.11 MPa^{-1}. Furthermore, the low-pressure sensing below 10 kPa could be realized by a decreasing cross-sectional area of MQW nanopillars. Therefore, our pillar array can provide wide applications for pressure sensing distribution through the design and optimization of three-dimensional (3D) array devices.

In order to obtain the dynamic PL imaging for pressure/strain distribution, the convex patterned BINN stamp manipulated by mechanical motions was used to provide dynamic pressure/strain for the MQW nanopillar array. Figure 4a gives the bright-field imaging of the BINN stamp in contact with our array device. These two parts are clearly observed from the backside of the transparent sapphire substrate. From optical morphology, it further shows a highly ordered alignment of dark dots corresponding to the InGaN/GaN MQW nanopillars, which is much better than the bottom-up grown nanowire arrays.[20,21] By cyclic pressing and releasing of the BINN stamp on the MQW array, dynamic PL imaging can be readily recorded for a pressure/strain evolution process from 0 to 14.94 MPa in Supporting Information, movie S1. The vertically dynamic response of pressure sensing corresponds to the real-time image changes of the patterned BINN stamp. Due to the ultrafast PL recombination process in nanoseconds or less,[29,30] it demonstrates unprecedented fast response for dynamic pressure/strain sensing, providing and guaranteeing very good time resolution of mechanical motions. Also, after 1000 pressing/releasing cycles, no degradation occurs in the pressure-sensitive PL imaging, exhibiting a good reliability and mechanical robustness of our array device, as shown in Figure S2.

Meanwhile, the static PL images of the MQW nanopillar array under external pressure/stresses of 0, 1.87, 7.47, and 14.94 MPa were directly obtained by a chromatic CCD camera, as shown in Figure 4b−e. By optical excitation, each InGaN/GaN MQW nanopillar could emit bright blue light without applied pressure. With increased compressive stress by pressing the BINN stamp, the PL intensity of the compressed pixels gradually decreased, while that of the noncompressed ones did not have any change. Based on the excellent pressure sensitivity, our InGaN/GaN MQW array can map the magnitude and spatial distribution of the applied pressure/strain on it. Figure 4b−e intuitively presents a series of high-resolution pressure images of the BINN logo under different compressive stresses. As the pressure increases, the patterned BINN logo

became more and more distinct. Similar results were also obtained by other stamps with the "PYC" pattern in Supporting Information, Figure S3. Furthermore, the 2D PL intensity difference images ($\Delta L = |L_\sigma(x,y) - L_0(x,y)|$) can be derived from the PL intensity maps by numerical subtraction. The processed images for 2D distribution of ΔL demonstrate the pressure/strain modulation effect on the PL intensity of InGaN/GaN MQW nanopillars, which are presented in Figure 4f–h.

Finally, to further demonstrate its capability and versatility for pressure/strain sensing, laterally dynamic PL imaging was carried out to record in real time the movement track of a personal signature, as depicted in Supporting Information, movie S2. First, a rectangle SU-8 stamp, just like a pen point, was pressed on the InGaN/GaN pillar array with a compressive stress of 3 MPa. Then, we load a lateral motion to the pen point by 3D micromanipulation stages while keeping its vertical height constant. The full trajectory of its movement clearly outlines the signature symbol "2", as shown in Supporting Information, Figure S4. Based on the dynamic PL imaging technique, many useful messages with a personal signature are included, such as shape, stroke, speed, and strength, which enable the development of personal signature recognition, identity authentication, psychological/physiological state monitoring, individualized encryption, and so on.

The piezo-phototronic effect offers a new way to modulate/control carrier generation, transport, separation, and recombination in light-emitting diodes or solar cells[22−28] by using pressure-induced piezoelectric charge. Here we find that such a piezoelectric charge can be used to tune photoluminescence under small pressure/strain for the first time. When pressure/strain are applied to the uniaxial GaN-based multilayer pillar, the piezoelectric polarization charges will be newly generated at its two ends due to a lack of central symmetry in wurtzite structures. Correspondingly, the PL optoelectronic processes, such as excitation and recombination, will be influenced by pressure/strain-induced piezoelectric charges at the interface. Figure 5 presents the schematic band diagram of the uniaxial n-GaN/(InGaN/GaN MQW)/p-AlGaN/p-GaN pillar (a) with and (b) without pressure/strain, simulated by SiLENse 5.4 software. No external bias voltage in the PL process is taken into account. In the equilibrium state, the n-GaN and p-AlGaN Fermi levels are equal ($E_{fn,n\text{-}GaN} = E_{fp,p\text{-}AlGaN}$) under no pressure/strain in Figure 5b. The built-in electric field in the p−n junction region will partially deplete the free carriers of InGaN QWs near the p-AlGaN layer. In addition, it will be directly tuned by the newly generated piezo-polarization field

$$eV_{piezo} = E^{\sigma}_{fp,p\text{-}AlGaN} - E^{\sigma}_{fn,n\text{-}GaN} \quad (2)$$

which depends on the applied pressure/strain σ on the InGaN/GaN MQW pillar in Figure 5a. When the

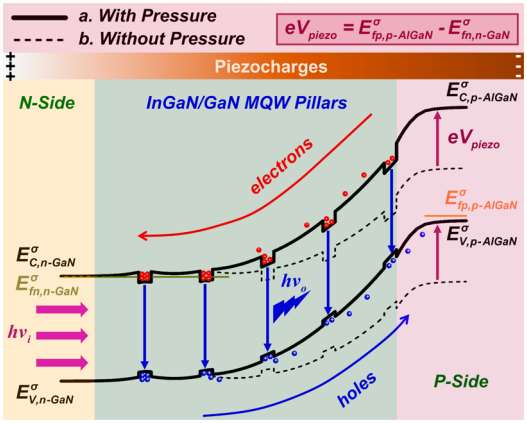

Figure 5. Mechanism of piezo-phototronic effect tuned PL. (a,b) Schematic band diagram of the uniaxial n-GaN/(InGaN/GaN MQW)/p-AlGaN/p-GaN pillar with and without pressure/strain, respectively.

[0001]-polarity InGaN/GaN MQW pillar is under compressive strain, the negative and positive ionic charges are created at the top p-AlGaN and bottom n-GaN, respectively. The compressive strain-induced piezopotential along a MQW pillar is equivalent to producing a reverse bias voltage on it. So, both the built-in electric field and depletion region width are increased, as shown in Figure 5a.[33] When the MQW pillar is illuminated by an excitation light of 405 nm, the photogenerated electron−hole pairs will be quickly separated by the increased built-in electric field, resulting in the decrease of radiative recombination probability and hence the PL intensity.

CONCLUSIONS

In summary, we have developed a new method of pressure sensing by using pressure/strain-induced piezoelectric charge to tune the PL intensity of InGaN/GaN MQWs under a small strain (0−0.15%). Such a modulation effect is distinct, linear, and ultrafast. On this basis, an all-optical pressure sensor array by the piezo-phototronic effect has been developed to measure dynamic pressure distribution without the need for electricity. Beyond the limitations of an electrical connection, our all-optical device offers a novel and suitable method for large-area, highly uniform, high-resolution, ultra-high-speed pressure/strain distribution sensing in top-down fabricated InGaN/GaN MQW nanopillar arrays. The pressure tuned PL imaging does not have any cross-talk. It can provide a wide range of applications for low-, medium-, or high-pressure regimes through the design and optimization of a 3D array structure. Meanwhile, the ultrafast PL imaging guarantees dynamic pressure distribution in real time. Furthermore, both the input signal and the output PL signal are all-optical with wide wavelength tunability from ultraviolet to infrared. It is beneficial for on-chip photonic integration in optical manipulating, transmitting, communicating, and recording, enabling a

great development of smart sensing, next-generation touch-pad technology, human−machine interfacing, micro/nano-opto-electromechanical systems, biomechanical imaging/analysis, and so on.

METHODS

Top-Down Fabrication of InGaN/GaN MQW Nanopillar Arrays. The blue $In_{0.18}Ga_{0.82}N$/GaN MQW multilayer was grown on a *c*-plane bipolished sapphire substrate by a low-pressure metal organic chemical vapor deposition system. From bottom to top, it consisted of a 2 μm undoped GaN buffer layer, a 3 μm n-type GaN layer, five periods of $In_{0.18}Ga_{0.82}N$/GaN (3 nm/12 nm) quantum well active layers, a 60 nm p-type $Al_{0.15}Ga_{0.85}N$ electron blocking layer, and a 100 nm p-type Mg-doped GaN capped layer.[22] The gallium, indium, and nitrogen sources were trimethylgallium (TMGa), trimethylindium (TMIn), and ammonia (NH_3), respectively. Biscyclopentadienyl magnesium (CP_2Mg) and silane (SiH_4) were used as the p-type and n-type doping sources, respectively. Vertically aligned InGaN/GaN MQW pillar arrays were fabricated as follows. First, a large-area and high-density dot matrix, with a diameter of 0.8 μm and a period of 4 μm, was photolithography patterned by a Nikon NSR1755i7A stepper machine. Ni−metal was used as the etching hard mask by electron-beam evaporation and lift-off processes. Then, the MQW nanopillar array was regularly formed using a low-damage inductively coupled plasma (ICP, SENTECH SI500) etching technique, the height of which was 1.2 μm for the physical separation of each MQW active region. The ICP etching process is based on chlorine (Cl_2) and boron trichloride (BCl_3) mixed gases with 30 and 3 sccm, respectively. After that, the remnant Ni−metal mask was removed by sulfuric acid, hydrogen peroxide, and deionized water mixed solution (its concentration ratio is $H_2SO_4/H_2O_2/H_2O$ = 3:1:10) for 30 s. Rapid thermal annealing at 350 °C for 1 min was implemented to repair the sidewall damage and defects. Subsequently, a 2.5 μm thick PMMA (Microchem) was spin-coated to wrap around the MQW pillars. The tips of the MQW pillars were exposed by oxygen plasma etching the top part of the PMMA.

High-Resolution PL Imaging from InGaN/GaN MQW Nanopillar Arrays. The pressure-modulated PL imaging measurement was based on an inverted confocal PL microscopy (Leica SP8), 3D micromanipulation stages, and a force gauge. A normal force/strain was applied on the MQW pillar arrays using a homemade stamp (a sapphire substrate with a convex character pattern of BINN in context or PYC in Supporting Information molded on it). The 3D micromanipulation stages could precisely adjust the position and pressure of the patterned stamps. The applied force could be controlled step by step with a given amount. According to the schematic diagram of the PL imaging measurement, we chose a semiconductor laser of 405 nm as the PL excitation source. The incident photons can penetrate through the bipolished sapphire substrate and GaN and AlGaN thin films and are only absorbed by $In_{0.18}Ga_{0.82}N$ QW active layers. The emitting PL signals of the ordered array were focused again and detected by a thermoelectrically cooled CCD and PL spectrum analysis. The PL measurement was performed at room temperature. Under different force/strain conditions, we mainly focused on the relative change in the emitted PL intensity. The PL spatial uniformity and intensity distribution of our array can be directly obtained. Importantly, the dynamic PL imaging under a 3D moving stamp was carried out to record tactile action and personal signature.

Conflict of Interest: The authors declare no competing financial interest.

Acknowledgment. This work was supported by NSFC (51472056, 51402064), Beijing Municipal NSF (7132121), the "thousands talents" program for pioneer researcher and his innovation team, China, and the Recruitment Program of Global Youth Experts, China.

Supporting Information Available: More detailed information about the pressure sensor structure; the stability and reproducibility of the sensor array; pressure-sensitive images of the pillar array under a PYC stamp; three-dimensional dynamic pressure sensing by PL imaging. This material is available free of charge *via* the Internet at http://pubs.acs.org.

REFERENCES AND NOTES

1. Mannsfeld, S. C. B.; Tee, B. C. K.; Stoltenberg, R. M.; Chen, C. V. H. H.; Barman, S.; Muir, B. V. O; Sokolov, A. N.; Reese, C.; Bao, Z. N. Highly Sensitive Flexible Pressure Sensors with Microstructured Rubber Dielectric Layers. *Nat. Mater.* **2010**, *9*, 859–864.
2. Takei, K.; Takahashi, T.; Ho, J. C.; Ko, H.; Gillies, A. G.; Leu, P. W.; Fearing, R. S.; Javey, A. Nanowire Active-Matrix Circuitry for Low-Voltage Macroscale Artificial Skin. *Nat. Mater.* **2010**, *9*, 821–826.
3. Gong, S.; Schwalb, W.; Wang, Y. W.; Chen, Y.; Tang, Y.; Si, J.; Shirinzadeh, B.; Chen, W. L. A Wearable and Highly Sensitive Pressure Sensor with Ultrathin Gold Nanowires. *Nat. Commun.* **2014**, *5*, 3132.
4. Lipomi, D. J.; Vosgueritchian, M.; Tee, B. C. K.; Hellstrom, S. L.; Lee, J. A.; Fox, C. H.; Bao, Z. N. Skin-like Pressure and Strain Sensors Based on Transparent Elastic Films of Carbon Nanotubes. *Nat. Nanotechnol.* **2011**, *6*, 788–792.
5. Someya, T.; Sekitani, T.; Kato, Y.; Kawaguchi, H.; Sakurai, T. A Large-Area, Flexible Pressure Sensor Matrix with Organic Field-Effect Transistors for Artificial Skin Applications. *Proc. Natl. Acad. Sci. U.S.A.* **2004**, *101*, 9966–9970.
6. Sekitani, T.; Yokata, T.; Zschieschang, U.; Klauk, H.; Bauer, S.; Takeuchi, K.; Takamiya, M.; Sakurai, T.; Someya, T. Organic Nonvolatile Memory Transistors for Flexible Sensor Arrays. *Science* **2009**, *326*, 1516.
7. Wu, W. Z.; Wen, X. N.; Wang, Z. L. Taxel-Addressable Matrix of Vertical-Nanowire Piezotronic Transistors for Active/Adaptive Tactile Imaging. *Science* **2013**, *340*, 952.
8. Wang, C.; Hwang, D.; Yu, Z. B.; Takei, K.; Park, J.; Chen, T.; Ma, B. W.; Javey, A. User-Interactive Electronic Skin for Instantaneous Pressure Visualization. *Nat. Mater.* **2013**, *12*, 899.
9. Pan, C. F.; Dong, L.; Zhu, G.; Niu, S. M.; Yu, R. M.; Yang, Q.; Liu, Y.; Wang, Z. L. High-Resolution Electroluminescent Imaging of Pressure Distribution Using a Piezoelectric Nanowire LED Array. *Nat. Photonics* **2013**, *7*, 752–758.
10. Nozaki, K.; Tanabe, K.; Shinya, A.; Matsuo, S.; Sato, T.; Taniyama, H.; Notomi, M. Sub-Femtojoule All-Optical Switching Using a Photonic-Crystal Nanocavity. *Nat. Photonics* **2010**, *4*, 477.
11. Piccione, B.; Cho, C. H.; Vugt, L. K. V.; Agarwal, R. All-Optical Active Switching in Individual Semiconductor Nanowires. *Nat. Nanotechnol.* **2012**, *7*, 640.
12. Kuramochi, E.; Nozaki, K.; Shinya, A.; Takeda, K.; Sato, T.; Matsuo, S.; Taniyama, H.; Sumikura, H.; Notomi, M. Large-Scale Integration of Wavelength-Addressable All-Optical Memories on a Photonic Crystal Chip. *Nat. Photonics* **2014**, *8*, 474.
13. Nozaki, K.; Shinya, A.; Matsuo, S.; Suzaki, Y.; Segawa, T.; Sato, T.; Kawaguchi, Y.; Takahashi, R.; Notomi, M. Ultralow-Power All-Optical RAM Based on Nanocavities. *Nat. Photonics* **2012**, *6*, 248.
14. Husko, C.; Rossi, A. D.; Combrie, S.; Tran, Q. V.; Raineri, F.; Wong, C. W. Ultrafast All-Optical Modulation in GaAs Photonic Crystal Cavities. *Appl. Phys. Lett.* **2009**, *94*, 021111.
15. Schonenberger, S.; Stoeferle, T.; Moll, N.; Mahrt, R. F.; Dahlem, M. S.; Wahlbrink, T.; Bolten, J.; Mollenhauer, T.; Kurz, H.; Offrein, B. J. Ultrafast All-Optical Modulator with Femtojoule Absorbed Switching Energy in Silicon-on-Insulator. *Opt. Express* **2010**, *18*, 22485.
16. Slavik, R.; Parmigiani, F.; Kakande, J.; Lundstrom, C.; Sjodin, M.; Andrekson, P. A.; Weerasuriya, R.; Sygletos, S.; Ellis, A. D.;

Gruner-Nielsen, L.; et al. All-Optical Phase and Amplitude Regenerator for Next-Generation Telecommunications Systems. *Nat. Photonics* **2010**, *4*, 690.
17. Suslov, S. S.; Bougrov, V. E.; Odnoblyudov, M. A.; Romanov, A. E. Modelling and Optimization of Electric Current Spreading in III-Nitride LEDs. *Phys. Status Solidi C* **2012**, *9*, 1105.
18. Süess, M. J.; Geiger, R.; Minamisawa, R. A.; Schiefler, G.; Frigerio, J.; Chrastina, D.; Isella, G.; Spolenak, R.; Faist, J.; Sigg, H. Analysis of Enhanced Light Emission from Highly Strained Germanium Microbridges. *Nat. Photonics* **2013**, *7*, 466–472.
19. Signorello, G.; Loertscher, E.; Khomyakov, P. A.; Karg, S.; Dheeraj, D. L.; Gotsmann, B.; Weman, H.; Riel, H. Inducing a Direct-to-Pseudodirect Bandgap Transition in Wurtzite GaAs Nanowires with Uniaxial Stress. *Nat. Commun.* **2014**, *5*, 3655.
20. Huang, C. T.; Song, J. H.; Lee, W. F.; Ding, Y.; Gao, Z. Y.; Hao, Y.; Chen, L. J.; Wang, Z. L. GaN Nanowire Arrays for High-Output Nanogenerators. *J. Am. Chem. Soc.* **2010**, *132*, 4766.
21. Chen, C. Y.; Zhu, G.; Hu, Y. F.; Yu, J. W.; Song, J. H.; Chen, K. Y.; Peng, L. H.; Chou, L. J.; Wang, Z. L. Gallium Nitride Nanowire Based Nanogenerators and Light-Emitting Diodes. *ACS Nano* **2012**, *6*, 5687.
22. Peng, M. Z.; Zhang, Y.; Liu, Y. D.; Song, M.; Zhai, J. Y.; Wang, Z. L. Magnetic-Mechanical-Electrical-Optical Coupling Effects in GaN-Based LED/Rare-Earth Terfenol-D Structures. *Adv. Mater.* **2014**, *26*, 6767–6772.
23. Wang, Z. L. Piezopotential Gated Nanowire Devices: Piezotronics and Piezo-phototronics. *Nano Today* **2010**, *5*, 540.
24. Wang, Z. L. Progress in Piezotronics and Piezo-phototronics. *Adv. Mater.* **2012**, *24*, 4632.
25. Wang, Z. L.; Yang, R. S.; Zhou, J.; Qin, Y.; Xu, C.; Hu, Y. F.; Xu, S. Lateral Nanowire/Nanobelt Based Nanogenerators, Piezotronics and Piezo-phototronics. *Mater. Sci. Eng. R* **2010**, *70*, 320.
26. Wang, Z. L. *Piezotronics and Piezo-Phototronics*; Springer: Berlin, 2013.
27. Yang, Q.; Wang, W. H.; Xu, S.; Wang, Z. L. Enhancing Light Emission of ZnO Microwire-Based Diodes by Piezo-phototronic Effect. *Nano Lett.* **2011**, *11*, 4012.
28. Yang, Q.; Liu, Y.; Pan, C. F.; Chen, J.; Wen, X. N.; Wang, Z. L. Largely Enhanced Efficiency in ZnO Nanowire/p-Polymer Hybridized Inorganic/Organic Ultraviolet Light-Emitting Diode by Piezo-phototronic Effect. *Nano Lett.* **2013**, *13*, 607.
29. Chin, A. H.; Ahn, T. S.; Li, H. W.; Vaddiraju, S.; Bardeen, C. J.; Ning, C. Z.; Sunkara, M. K. Photoluminescence of GaN Nanowires of Different Crystallographic Orientations. *Nano Lett.* **2007**, *7*, 626.
30. Li, C.; Stokes, E. B.; Hefti, R.; Moyer, P.; Armour, E. A.; Arif, R.; Byrnes, D.; Lee, S. M.; Papasouliotis, G. D. PL Spatial Variation in InGaN/GaN MQWs Studied by Confocal Microscopy and TRPL Spectroscopy. *ECS J. Solid State Sci. Technol.* **2013**, *2*, R262.
31. Chang, H. J.; Hsieh, Y. P.; Chen, T. T.; Chen, Y. F.; Liang, C. T.; Lin, T. Y.; Tseng, S. C.; Chen, L. C. Strong Luminescence from Strain Relaxed InGaN/GaN Nanotips for Highly Efficient Light Emitters. *Opt. Express* **2007**, *15*, 9357.
32. Boland, J. J. Flexible Electronics within Touch of Artificial Skin. *Nat. Mater.* **2010**, *9*, 790.
33. Liu, Y.; Niu, S. M.; Yang, Q.; Klein, B. D. B.; Zhou, Y. S.; Wang, Z. L. Theoretical Study of Piezo-phototronic Nano-LEDs. *Adv. Mater.* **2014**, *26*, 72090.